

Journal of Materials Chemistry A

Materials for energy and sustainability

Accepted Manuscript

This article can be cited before page numbers have been issued, to do this please use: Y. Son, H. Jang, B. Wen, C. Jo, A. Groombridge, A. Boies, M. G. Kim and M. De Volder, *J. Mater. Chem. A*, 2025, DOI: 10.1039/D4TA08141B.



This is an Accepted Manuscript, which has been through the Royal Society of Chemistry peer review process and has been accepted for publication.

Accepted Manuscripts are published online shortly after acceptance, before technical editing, formatting and proof reading. Using this free service, authors can make their results available to the community, in citable form, before we publish the edited article. We will replace this Accepted Manuscript with the edited and formatted Advance Article as soon as it is available.

You can find more information about Accepted Manuscripts in the [Information for Authors](#).

Please note that technical editing may introduce minor changes to the text and/or graphics, which may alter content. The journal's standard [Terms & Conditions](#) and the [Ethical guidelines](#) still apply. In no event shall the Royal Society of Chemistry be held responsible for any errors or omissions in this Accepted Manuscript or any consequences arising from the use of any information it contains.

ARTICLE

Compositional Study of Ti-Nb Oxide (TiNb₂O₇, Ti₂Nb₁₀O₂₉, Ti₂Nb₁₄O₃₉, and TiNb₂₄O₆₂) Anode for High Power Li Ion BatteriesYeonguk Son^{a,b,†}, Haeseong Jang^{c,†}, Bo Wen^a, Changshin Jo^d, Alexander S Groombridge^e, Adam Boies^f, Min-Gyu Kim^{g,*}, Michael De Volder^{a,*}Received 00th January 20xx,
Accepted 00th January 20xx

DOI: 10.1039/x0xx00000x

Titanium niobium oxides (TNOs) are attractive anode materials for high power density Li-ion batteries. However, the details of capacity storage in TNOs is not fully understood today as it depends on the Ti and Nb composition and their changes in oxidation state. This is further complicated by a wide variation in gravimetric capacities reported in literature for TNO anodes. Therefore, in this work, we systematically synthesise TiNb₂O₇, Ti₂Nb₁₀O₂₉, Ti₂Nb₁₄O₃₉, and TiNb₂₄O₆₂ particles using the same solid state reaction approach, and report their electrochemical properties via galvanostatic cycling, cyclic voltammetry, galvanostatic intermittent titration technique (GITT). Further we use *operando* X-ray absorption spectroscopy (XAS) to investigate the redox reactions taking place in each of these compositions, which provides new insights in their charge storage mechanisms. We found that of the materials tested, TiNb₂O₇ anodes have the best cycling and rate performance, which could be related to the higher utilization of Nb redox revealed via *operando* XAS analysis.

Introduction

Lithium titanium oxide (LTO) is a commercially used anode materials for high power lithium-ion batteries (LIBs) [1]. Although the gravimetric capacity (~175 mAh/g) and nominal voltage of LTO (~1.55 V) are worse than those of commercial graphite anodes (360 mAh/g and 0.1 V respectively), LTO anodes have a superior rate performance, which is favourable for high power application [2]. Hence, there have been many publications showing LTO anodes with great capacity retention, even at 10 C-rates with high material areal loadings [3]. In contrast, graphite anodes are typically limited in rate performance, which is in part due to its very low nominal voltage versus Li, which can lead to Li plating. The development of new LIB anodes for electric vehicles (EVs) needs to accommodate the requirements for a long driving range with those of short battery charging times and battery safety. It is therefore important to balance the parameters such as the

anode capacity, nominal voltage, rate performance and cost judiciously. LTO anodes were used in EVs such as Mitsubishi's i-MiEV and Honda's Fit EV, as well as power tools, despite their low capacity and high nominal voltage, as described above [1]. However, most EVs have graphite anodes, and many manufacturers are exploring alternative materials that combine the rate performance of LTO with the capacity of graphite, which are promising for improving future EV batteries. Recently, titanium niobium oxide (TNO) has gained interest as one such material [4–8].

The gravimetric capacity of reported TNO anodes ranges from 210 to 341 mAh/g depending on the material design and cut-off voltage, which is 20~95% higher than LTO anodes, while maintaining fast charging properties [5,9]. However, the exact details of the redox mechanisms contributing to the gravimetric capacity measure in TNO anodes remain ambiguous. For example, Dr. S. Dai and co-workers reported valance state variation of Ti and Nb during the initial discharge by *in situ* Ti K-edge and Nb K-edge X-ray absorption near edge structure (XANES) spectra between 1.0 V and 3.0 V voltage range in TiNb₂O₇ [10]. As a result, Ti⁴⁺ and Nb⁵⁺ were reduced to Ti^{3.2+} and Nb^{3.6+}, which well matched with experimental discharge capacity of 281 mAh/g. However, it could not explain the broad range of capacities reported in the publications. Moreover, there are only a few reports investigating how redox mechanisms vary depending on the TNO formulation [11,12]. In this work, we investigate the reaction mechanisms taking place in TNO anodes by systematically synthesising materials with different compositions (TiNb₂O₇, Ti₂Nb₁₀O₂₉, Ti₂Nb₁₄O₃₉, and TiNb₂₄O₆₂) using the same synthesis protocol and benchmarking them against LTO anodes. We developed a dry solid state synthesis method for the above four TNO formulations which

^a Department of Engineering, University of Cambridge, 17 Charles Babbage Road, CB3 0FS Cambridge, UK. E-mail: mfld2@cam.ac.uk

^b Department of Chemical Engineering, Changwon National University, Changwon, Gyeongsangnam-do 51140, Republic of Korea

^c Department of Advanced Materials Engineering, Chung-Ang University, 4726, Seodong-daero, Daedeok-myeon, Anseong, Gyeonggi-do 17546, the Republic of Korea

^d Graduate Institute of Ferrous and Energy Materials Technology (GIFT), Pohang University of Science and Technology (POSTECH), 77 Cheongam-Ro, Nam-Gu, Pohang, Gyeongbuk, 37673, Republic of Korea

^e Echion Technologies Ltd, Unit 9, Cambridge South, West Way, CB22 3FG Cambridge, UK

^f Department of Mechanical Engineering, Stanford University, Stanford, CA 94305

^g Beamline Research Division, Pohang Accelerator Laboratory (PAL), Pohang 37673, Republic of Korea. E-mail: habga82@postech.ac.kr

† These authors contributed equally to this work.

Supplementary Information available: [details of any supplementary information available should be included here]. See DOI: 10.1039/x0xx00000x



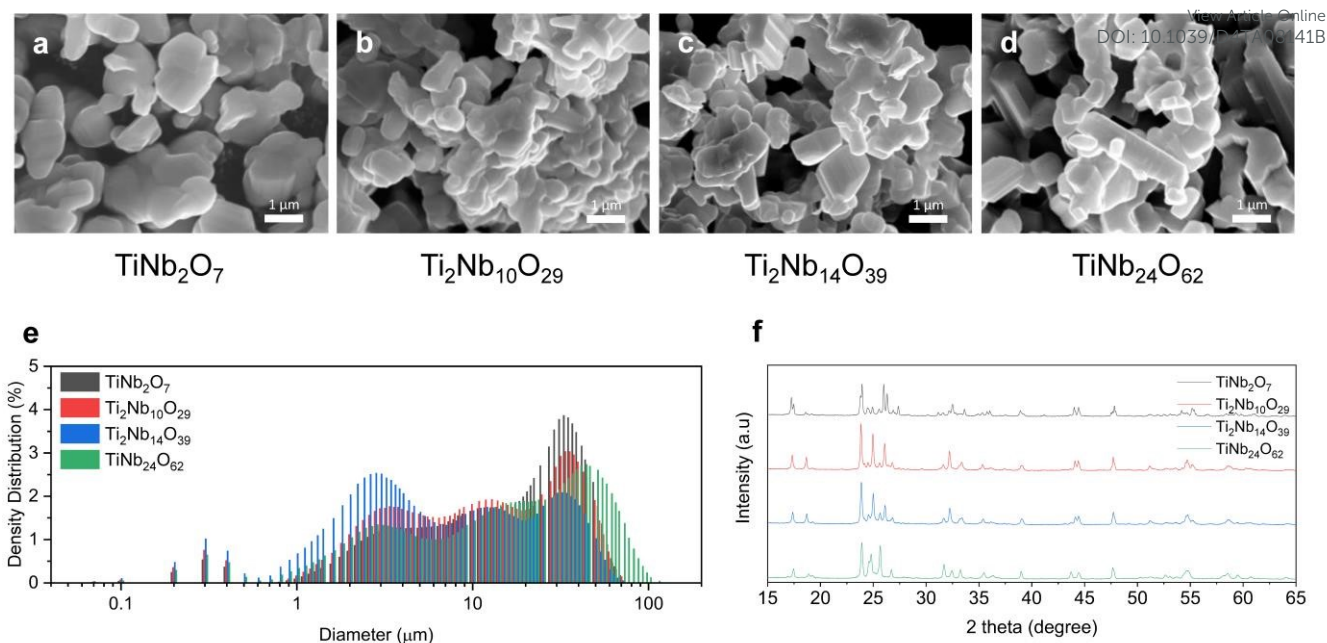


Figure 1. Morphology and crystalline structures of the as-prepared TNOs: SEM images of (a) TiNb_2O_7 , (b) $\text{Ti}_2\text{Nb}_{10}\text{O}_{29}$, (c) $\text{Ti}_2\text{Nb}_{14}\text{O}_{39}$, and (d) $\text{TiNb}_{24}\text{O}_{62}$, (e) PSD results, and (f) power XRD patterns of TNOs

allows for a side-by-side comparison of their capacity, rate performance, capacity retention and capacitive behavior. Further, in order to study the charge storage mechanisms taking place in these materials, detailed electrochemical tests are carried out together with *operando* XAS to track the changes in redox state of Ti and Nb as a function of the state of charge. These new fundamental insights in the operation of different TNO batteries are critical for their further optimisation and potential use in future EVs and other commercial applications.

Results and discussion

We synthesized 4 different compositions of TNO (TiNb_2O_7 , $\text{Ti}_2\text{Nb}_{10}\text{O}_{29}$, $\text{Ti}_2\text{Nb}_{14}\text{O}_{39}$, and $\text{TiNb}_{24}\text{O}_{62}$) via solid state reactions. We blended TiO_2 and NbO_2 powders with a blade mixer and calcinated them at 1000°C under oxygen atmosphere. A detailed description of the synthesis process is provided in the experimental section. The resulting shape and size of the four TNO compositions is shown in Figures 1 and S1, and show a similar spread of diameters, which therefore allow for a fair direct comparison of their electrochemical performance. The crystalline structure of TNO materials is based on ReO_3 -type crystal building blocks, which are formed by corner- and/or edge-sharing octahedra and a small number of tetrahedra [11]. To verify the crystalline structure of 4 different compositions of TNO, XRD analysis and Rietveld refinement were carried out (Figure 1f and S2). The Rietveld refinement results shown in Figure S2 match with previous reports, which validates the synthesis protocol developed in this work [13–16]. Details of the refined lattice parameters are summarized in table S1 [17–19]. TiNb_2O_7 , $\text{Ti}_2\text{Nb}_{10}\text{O}_{29}$, and $\text{TiNb}_{24}\text{O}_{62}$ are constructed with structural unit of a corner- and edge-shared 3×3 octahedron block (space group $C2/m$), 3×4 octahedron block (space group

$A2/m$), and 3×4 octahedron block plus 0.5 tetrahedron at the block corner (space group $C2$) respectively [20]. All the other compositions of Ti-Nb oxides studied here have a single phase except TiNb_2O_7 which has mixed phase of TiNb_2O_7 (82.04%) and H phase Nb_2O_5 (17.96%). The Ti and Nb are homogeneously mixed in the Ti-Nb oxide structures because the ionic radii of Ti^{4+} and Nb^{5+} are similar (0.61 \AA for Ti^{4+} and 0.64 \AA for Nb^{5+}) [21].

The energy storage in TNO anode is driven by changes in oxidation states of Ti and Nb during charge and discharge. According to previous reports, Ti^{4+} and Nb^{5+} are converted to Ti^{3+} and Nb^{3+} during charging (lithiation) process [11]. The theoretical capacities of TNO anodes depend on the composition of Ti and Nb and can be calculated by assuming certain oxidation state change and normalising the charges stored per unit mass. We carried out these calculations (see supporting information for details) under different assumptions:

- (i) Ti^{4+} and Nb^{5+} are converted entirely to Ti^{3+} and Nb^{3+} (One electron transfer in Ti, two electrons transfer in Nb): This results in theoretical capacities of 388 mAh/g for TiNb_2O_7 , of 396 mAh/g for $\text{Ti}_2\text{Nb}_{10}\text{O}_{29}$, of 398 mAh/g for $\text{Ti}_2\text{Nb}_{14}\text{O}_{39}$, and of 402 mAh/g for $\text{TiNb}_{24}\text{O}_{62}$.
- (ii) Ti^{4+} and Nb^{5+} are converted to Ti^{3+} and Nb^{4+} (One electron transfer in Ti, one electron transfer in Nb): This results in theoretical capacities of 233 mAh/g for TiNb_2O_7 , of 216 mAh/g for $\text{Ti}_2\text{Nb}_{10}\text{O}_{29}$, of 212 mAh/g for $\text{Ti}_2\text{Nb}_{14}\text{O}_{39}$, and of 205 mAh/g for $\text{TiNb}_{24}\text{O}_{62}$.

These calculations illustrate that the capacity of TNO anodes can vary substantially depending on the actual oxidation state changes that are achieved in Ti and Nb within the voltage



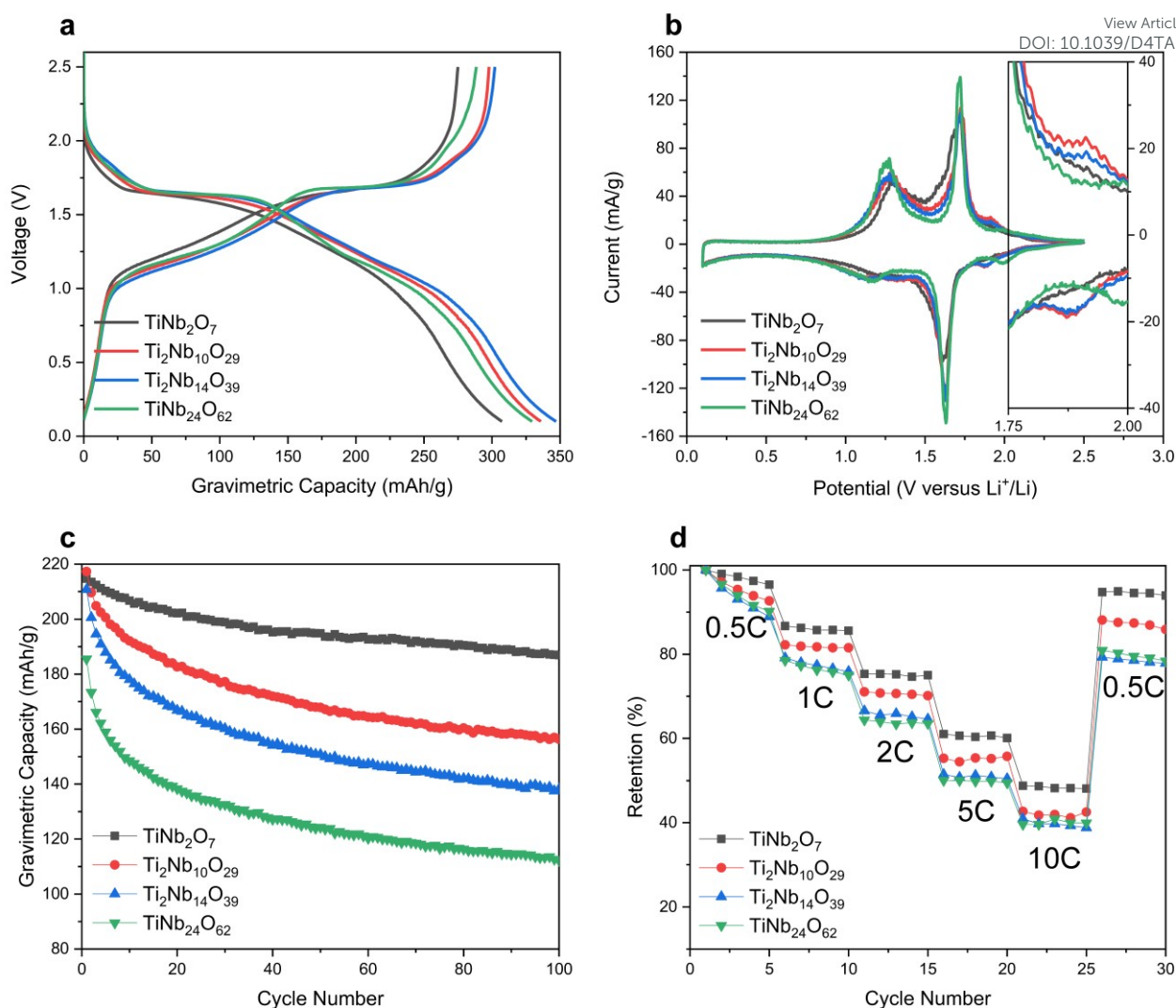


Figure 2. Electrochemical performance of the as-prepared TNO anodes: (a) 0.05C first formation voltage profiles of the TNO anodes, (b) 0.04 mV/s cyclic voltammetry (inset: magnified part from 1.75 to 2.00 V), (c) 0.5C cycling performances of the TNO anodes. (d) Rate performances of the TNO anodes

window they are cycled. It is worth noting that the capacities of TNO anode reported in previous publications vary broadly (210~326 mAh/g) and we have summarized these values in Table S2 [9,22–32].

We first carried out half-cell experiments in coin cells with active material: Carboxymethyl cellulose (CMC)/ Styrene butadiene rubber (SBR) binder: Super-P carbon additive weight ratio of 8:1:1 and are tested in triplicates. All electrodes were coated on a Cu foil with an areal loading of 1.5~2.0 mg/cm² and were tested using 1.3 M LiPF₆ in mixture of ethylene carbonate (EC), Ethyl methyl carbonate (EMC) and diethyl carbonate (DEC) (3:5:2) with 10 wt% fluoroethylene carbonate (FEC) as an electrolyte. Cut-off voltage was 0.1-2.5 V. Our TiNb₂O₇, Ti₂Nb₁₀O₂₉, Ti₂Nb₁₄O₃₉, and TiNb₂₄O₆₂ anodes show reversible capacities of 278, 299, 302, and 289 mAh/g respectively and coulombic efficiencies of 88.1, 88.7, 87.7 and 87.5% in first 0.05C formation cycle (Figure 2a and S3). The capacities measured fall between the two different oxidation state assumptions made above, and this warrants a more detailed

investigation of the actual changes in oxidation taking place. To confirm the extent and potentials of each redox reactions, cyclic voltammetry (CV) was performed at slow scan rate of 0.04 mV/s (figure 2b). The major lithiation and delithiation peaks of all the TNO compositions studied here are between 1.6 and 1.7 V vs. Li/Li⁺ respectively, which has previously been associated to the redox reactions of Nb⁵⁺/Nb⁴⁺ [33,34]. The second highest redox peak couple shows at around 1.1-1.3 V (lithiation) and 1.3 V (delithiation), which has been linked to the redox reactions of Nb⁴⁺/Nb³⁺. The lithiation peak of Nb⁴⁺/Nb³⁺ was broader than the delithiation peak of Nb⁴⁺/Nb³⁺. The minor peak couples at 1.8-2.0 V are related to the redox reactions of Ti⁴⁺/Ti³⁺ [22,31,35]. The redox peaks of Ti⁴⁺/Ti³⁺ at TiNb₂₄O₆₂ sample are at around 2.0 V and the redox peaks of Ti⁴⁺/Ti³⁺ at Ti₂Nb₁₀O₂₉ and Ti₂Nb₁₄O₃₉ show at around 1.9 V (see inset of Figure 2b). However, TiNb₂O₇ show no minor peaks at 1.8-2.0 V.

Figure 2c shows cycling performance of TNO anodes at 0.5C in half-cells. Of the TNO anodes studied here, the TiNb₂O₇ anode showed the best cycling performance of 87% retention at 100th



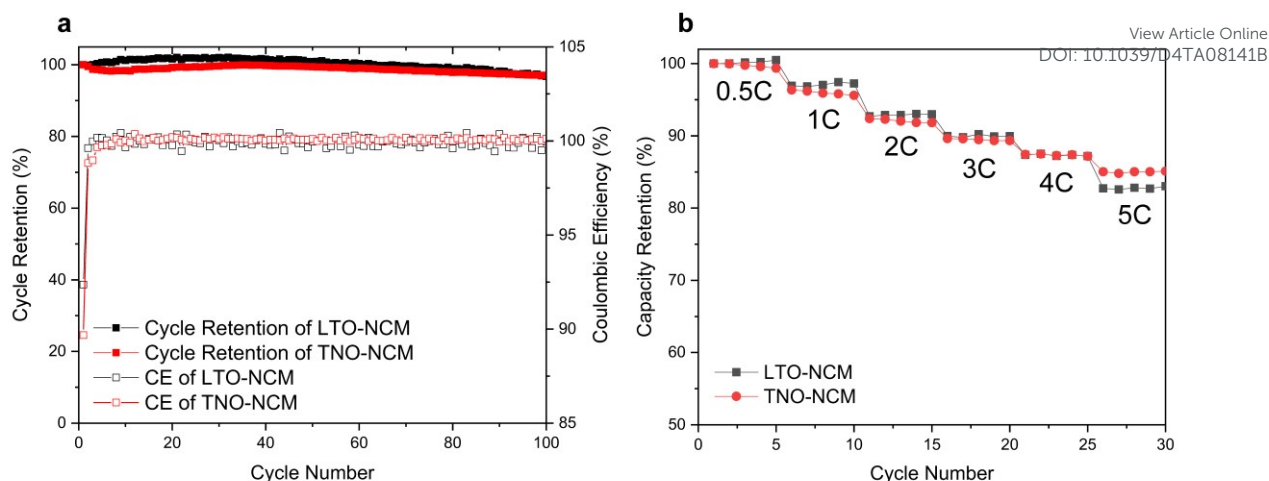


Figure 3. Full cell performance with TNO and LTO anode (a) cycling performance of LTO-NCM and TNO-NCM full cells. (b) Rate performance of LTO-NCM and TNO-NCM full cells

cycle. The $\text{Ti}_2\text{Nb}_{10}\text{O}_{29}$, $\text{Ti}_2\text{Nb}_{14}\text{O}_{39}$, and $\text{TiNb}_{24}\text{O}_{62}$ anodes show retentions of 72, 66, and 60% at 100th cycle respectively. TiNb_2O_7 anodes also show a better rate performance than other TNO anodes studied here. As shown in figure 2b, TiNb_2O_7 achieved a capacity retention of 48% at 10C whereas $\text{Ti}_2\text{Nb}_{10}\text{O}_{29}$, $\text{Ti}_2\text{Nb}_{14}\text{O}_{39}$ and $\text{TiNb}_{24}\text{O}_{62}$ both achieve about 42, 40 and 41% respectively. Note that in high-rate performance, slight differences in particle size may have an effect. However, in our experiments, the differences in electrochemical performance based on the Ti-to-Nb ratio in TNO anodes were not overshadowed by variations in particle size.

To verify the practical viability of our TNO anodes and to compare them with commercial LTO anodes, we compared the full cell performances of TNO and LTO anodes with same $\text{LiNi}_{0.6}\text{Co}_{0.2}\text{Mn}_{0.2}\text{O}_2$ (NCM622) cathode with N/P ratio of 1.4. We utilized the TiNb_2O_7 composition, which showed the best performance in our TNO anode half-cell tests, for the full cell experiments. Figure S4 shows voltage profiles of full cell formation cycles. Gravimetric capacity of full cell is based on the weight sum of both cathode and anode active materials. The discharge capacities and coulombic efficiencies of TNO-NCM and LTO-NCM full cells at 1st formation were 81.86 mAh/g and 91.41% (for TNO-NCM) and 74.13 mAh/g and 91.69% (for LTO-NCM) and respectively. Nominal voltages of TNO-NCM and LTO-NCM full cells at 1st discharge were 2.19 and 2.29 V respectively. The nominal voltage of TNO-NCM is slightly lower than that of LTO-NCM, however the gravimetric capacity is slightly higher. The cycling performances of both TNO-NCM and LTO-NCM full cells showed very stable 0.5C cycling life (figure 3a). There is no significant fading in cycling life. Also, two full cells show great rate performance at 0.5C charge and 0.5, 1, 2, 3, 4, and 5 C discharge rate test. At 5 C discharge rate, TNO-NCM and LTO-NCM full cells show a similar capacity retention of 85 and 83% respectively (figure 3b).

To measure the oxidation state changes of Nb directly, we used an *operando* XANES. Because of Ti's low threshold energy, *operando* XANES analysis is impossible because the photon energy corresponding to the Ti K-edge is almost entirely absorbed by the thick Cu foil. However, by measuring the actual

oxidation state change of Nb with XANES alongside the capacity, we can calculate the capacity contribution from Ti and infer its oxidation state change (see supporting information for the details of the calculation method). Figure 4a shows the Nb K-edge XANES absorption spectra of TNO anodes at fully lithiated and delithiated states and continuous spectra changes are provided in figure S5. Based on the results of XANES spectra and reference data, the oxidation number of Nb at TNO anode is obtained from a least-square method (LSM) (see Figure 4b). Note that we utilized Nb_2O_3 and Nb_2O_5 as Nb^{3+} and Nb^{5+} reference materials respectively in oxidation state measurement in XANES analysis [18]. During the delithiation process, the oxidation state changes of Nb in TiNb_2O_7 , $\text{Ti}_2\text{Nb}_{10}\text{O}_{29}$, $\text{Ti}_2\text{Nb}_{14}\text{O}_{39}$, and $\text{TiNb}_{24}\text{O}_{62}$ electrode are 1.64, 1.58, 1.59, and 1.43 respectively. The lower the ratio of Nb in TNO composition, the greater the electron transfer in Nb. In other words, the redox reaction of Nb is the most pronounced in TiNb_2O_7 and decreases with materials having a relatively higher Nb content. The calculated oxidation state changes of Ti at TiNb_2O_7 , $\text{Ti}_2\text{Nb}_{10}\text{O}_{29}$, $\text{Ti}_2\text{Nb}_{14}\text{O}_{39}$, and $\text{TiNb}_{24}\text{O}_{62}$ electrode are 0.31, 0.42, 0.20, and 0.87 respectively (figure S5). Note that Nb/Ti ratios in TiNb_2O_7 , $\text{Ti}_2\text{Nb}_{10}\text{O}_{29}$, $\text{Ti}_2\text{Nb}_{14}\text{O}_{39}$, and $\text{TiNb}_{24}\text{O}_{62}$ are 2, 5, 7, and 24 respectively.

Figure 4c, and d show the radial structure function of TNO samples obtained by Fourier transforms of the Nb K-edge EXAFS (Extended X-ray absorption fine structure) oscillations at fully lithiated and delithiated states. The continuous spectra changes are provided in figure S6. Because the EXAFS data is qualitative, we focused on identifying the differences between TNO compositions and distinct properties from previously reported Nb_2O_5 anodes [36]. The peaks at around 1.7-2.2 Å in the figure 4d corresponds to the Nb–O interaction and the peaks at around 2.8-3.5 Å in the figure 4d corresponds to the Nb–TM (transition metal) interaction. In all samples, the peaks of Nb–O interaction are characteristically higher than those of Nb–TM interaction in fully lithiated state, in contrast, the peaks of Nb–TM interaction are higher than those of Nb–O interaction in fully delithiated state. This phenomenon corresponds to the lithium-ion diffusion mechanism in tetragonal Nb_2O_5 anode [36].



This suggests that Li ions diffuse through the Nb-TM interlayer in TNO anodes similar to lithium-ion diffusion through Nb-Nb interlayer in tetragonal Nb₂O₅ anodes [36]. This is evidence that TiNb₂O₇, which has a higher O/Nb ratio compared to other TNO samples, can be advantageous in lithium-ion diffusion. In other words, the lower O/Nb ratio in TNO anodes, the lower the rate performance.

which suggest faster kinetics in TiNb₂O₇. Next, GITT (Galvanostatic Intermittent Titration Technique) was conducted to quantify both ohmic and non-ohmic overpotentials in different TNO compositions as a function of the state of charge (during lithiation) (see supporting information for detailed pulse method). The raw data of GITT data is shown in figure S8. Figure 5c show that the ohmic overpotentials range from 0.005-0.020

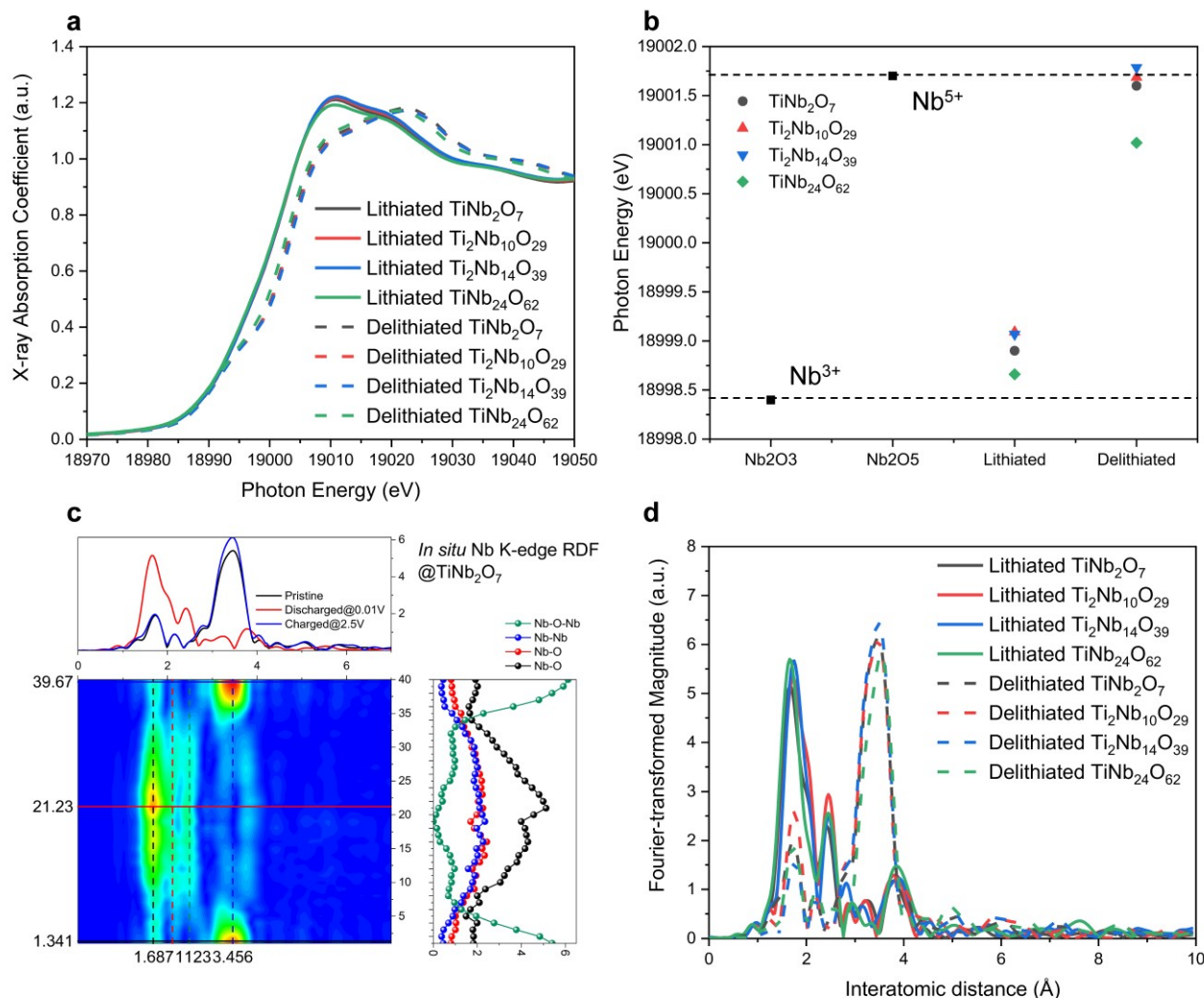


Figure 4. XANES and EXAFS analysis of the TNO anodes. (a) the Nb K-edge XANES absorption spectra of TNO anodes at fully lithiated and delithiated states (b) the oxidation number of Nb at TNO anode (c) EXAFS results of TiNb₂O₇, (d) Fourier transforms of the Nb K-edge EXAFS oscillations at fully lithiated and delithiated states

To verify this trend, we measure the diffusion properties of our different TNO anodes using a CV based method published previously [37,38]. Figure 5a shows the CV data for TiNb₂O₇ and the other TNO anodes are shown in figure S7. We plotted the log (sweep rate) versus log (peak current) graph to investigate the redox mechanism of TNO anodes (figure 5b). In this graph, if the slope is close to 1, there is no diffusion limit (capacitive behaviour), and if it is close to 0.5, it has general diffusion properties [37,38]. As shown in figure 5b, the slope values of TiNb₂O₇, Ti₂Nb₁₀O₂₉, Ti₂Nb₁₄O₃₉, and TiNb₂₄O₆₂ electrode are 0.89, 0.78, 0.76, and 0.65 respectively. The slope was the highest in TiNb₂O₇ anode and is decreasing with the oxygen to Nb and Ti ratio. This confirms the trend measured by EXAFS,

V. The non-ohmic drop are placed range of 0.00-0.45 V (figure 5d). The overpotential difference between samples was smaller than the overpotential difference according to SOC. Therefore, the rate performance of TNO anodes is determined more by diffusion than by the difference in overpotential.

Conclusions

In conclusion, we synthesised four classes of TNO anodes with different Nb and Ti contents (TiNb₂O₇, Ti₂Nb₁₀O₂₉, Ti₂Nb₁₄O₃₉, and TiNb₂₄O₆₂) using the same solid state synthesis method to obtain materials that can be compared directly. The different Ti and Nb compositions result in different



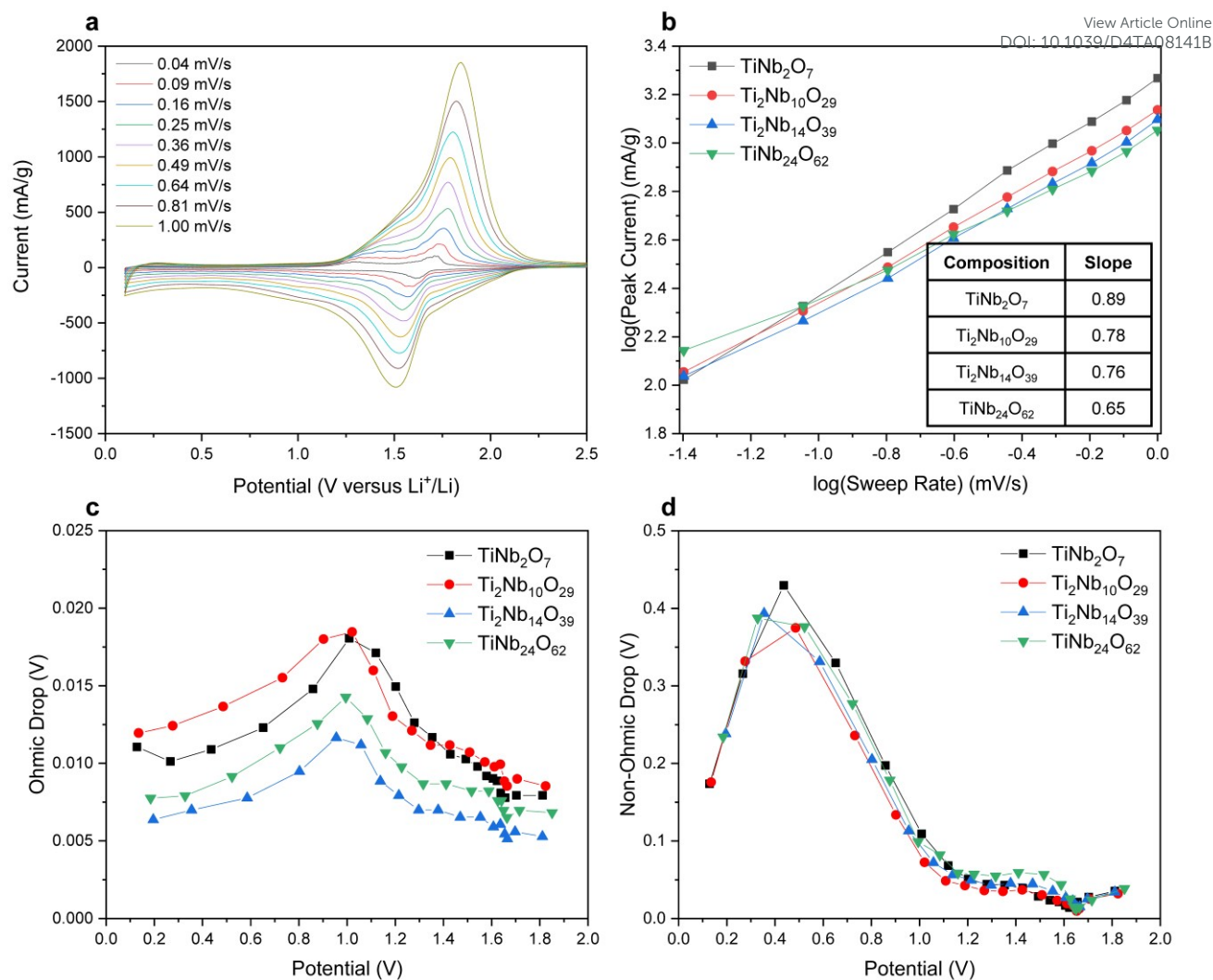


Figure 5. Electrochemical analysis of the TNO anodes (a) CV results of TiNb_2O_7 anode (scan rate: 0.04~1.00 mV/s), (b) log (sweep rate) versus. log (peak current) graph from CV results, (c) ohmic overpotentials derived by GITT results. (d) non-ohmic overpotentials derived by GITT results.

electrochemical performances. Among them, TiNb_2O_7 showed the lowest gravimetric capacity but the best cycling and rate performance. To understand these differences in performance, we measured the changes in oxidation state of Nb via *operando* XAS and calculate the changes in oxidation state of Ti. Interestingly, the oxidation state change of Nb in TiNb_2O_7 was greater than in our other TNO anodes. In other words, TiNb_2O_7 anode used the oxidation state of Nb more efficiently and rely less on changes in oxidation state of Ti. The increase in the Ti to Nb ratio in TNO anode seem to lead to the increases in gravimetric capacity, but at the cost of decreased cycling stability, providing new guidelines for material design. Similarly, we observed that the relative oxygen content of TNO anodes affects performance, where the higher O/Nb ratio demonstrated superior rate performance.

Author contributions

We strongly encourage authors to include author contributions and recommend using [CRediT](#) for standardised contribution descriptions.

Please refer to our general [author guidelines](#) for more information about authorship.

Conflicts of interest

In accordance with our policy on [Conflicts of interest](#) please ensure that a conflicts of interest statement is included in your manuscript here. Please note that this statement is required for all submitted manuscripts. If no conflicts exist, please state that "There are no conflicts to declare".

Data availability

A data availability statement (DAS) is required to be submitted alongside all articles. Please read our [full guidance on data availability statements](#) for more details and examples of suitable statements you can use.



Acknowledgements

Y.S. and H.J. contributed equally to this work. This research was funded by an ERC Consolidator Grant (MIGHTY-866005).

References

- [1] C. Lin, S. Yu, H. Zhao, S. Wu, G. Wang, L. Yu, Y. Li, Z.-Z. Zhu, J. Li, S. Lin, Defective Ti₂Nb₁₀O₂₇:1: an advanced anode material for lithium-ion batteries, 5 (2015) 17836. <https://doi.org/10.1038/srep17836>.
- [2] C. Lin, S. Yu, H. Zhao, S. Wu, G. Wang, L. Yu, Y. Li, Z.-Z. Zhu, J. Li, S. Lin, Defective Ti₂Nb₁₀O₂₇:1: an advanced anode material for lithium-ion batteries, 5 (2015). <https://doi.org/10.1038/srep17836>.
- [3] K. Ise, S. Morimoto, Y. Harada, N. Takami, Large lithium storage in highly crystalline TiNb₂O₇ nanoparticles synthesized by a hydrothermal method as anodes for lithium-ion batteries, 320 (2018) 7–15. <https://doi.org/10.1016/j.ssi.2018.02.027>.
- [4] C. Lin, S. Deng, D.J. Kautz, Z. Xu, T. Liu, J. Li, N. Wang, F. Lin, Intercalating Ti₂Nb₁₄O₃₉ Anode Materials for Fast-Charging, High-Capacity and Safe Lithium-Ion Batteries, 13 (2017) 1702903. <https://doi.org/10.1002/sml.201702903>.
- [5] X. Wang, G. Shen, Intercalation pseudo-capacitive TiNb₂O₇@carbon electrode for high-performance lithium ion hybrid electrochemical supercapacitors with ultrahigh energy density, 15 (2015) 104–115. <https://doi.org/10.1016/j.nanoen.2015.04.011>.
- [6] X. Xia, S. Deng, S. Feng, J. Wu, J. Tu, Hierarchical porous Ti₂Nb₁₀O₂₉ nanospheres as superior anode materials for lithium ion storage, 5 (2017) 21134–21139. <https://doi.org/10.1039/C7TA07229E>.
- [7] H. Park, H.B. Wu, T. Song, X.W. (David) Lou, U. Paik, Porosity-Controlled TiNb₂O₇ Microspheres with Partial Nitridation as a Practical Negative Electrode for High-Power Lithium-Ion Batteries, 5 (2015) 1401945. <https://doi.org/10.1002/aenm.201401945>.
- [8] X. Jin, Y. Deng, H. Tian, M. Zhou, W. Tang, H. Dong, X. Zhang, R. Liu, Homovalent doping: An efficient strategy of the enhanced TiNb₂O₇ anode for lithium-ion batteries, 9 (2023) 1257. <https://doi.org/10.1016/j.jee.2023.01.007>.
- [9] R. Schmich, R. Wagner, G. Hörpel, T. Placke, M. Winter, Performance and cost of materials for lithium-based rechargeable automotive batteries, 3 (2018) 267–278. <https://doi.org/10.1038/s41560-018-0107-2>.
- [10] A. Tolosa, S. Fleischmann, I. Grobelsek, A. Quade, E. Lim, V. Presser, Binder-Free Hybrid Titanium–Niobium Oxide/Carbon Nanofiber Mats for Lithium-Ion Battery Electrodes, 11 (2018) 159–170. <https://doi.org/10.1002/cssc.201701927>.
- [11] L. Hu, L. Luo, L. Tang, C. Lin, R. Li, Y. Chen, Ti₂Nb₂xO₄+5x anode materials for lithium-ion batteries: a comprehensive review, 6 (2018) 9799–9815. <https://doi.org/10.1039/c8ta00895g>.
- [12] C. Yang, S. Deng, C. Lin, S. Lin, Y. Chen, J. Li, H. Wu, Porous TiNb₂₄O₆₂ microspheres as high-performance anode materials for lithium-ion batteries of electric vehicles, 8 (2016) 18792–18799. <https://doi.org/10.1039/C6NR04992C>.
- [13] J. Gao, X. Cheng, S. Lou, Y. Ma, P. Zuo, C. Du, Y. Gao, G. Yin, Self-doping Ti_{1-x}Nb_{2+x}O₇ anode material for lithium-ion battery and its electrochemical performance, 728 (2017) 534–540. <https://doi.org/10.1016/j.jallcom.2017.09.045>.
- [14] K. Tang, X. Mu, P.A. van Aken, Y. Yu, J. Maier, “Nano-Pearl-String” TiNb₂O₇ as Anodes for Rechargeable Lithium Batteries, 3 (2013) 49–53. <https://doi.org/10.1002/aenm.201200396>.
- [15] K.J. Griffith, I.D. Seymour, M.A. Hope, M.M. Butala, L.K. Lamontagne, M.B. Preefer, C.P. Koçer, G. Henkelman, A.J. Morris, M.J. Cliffe, S.E. Dutton, C.P. Grey, Ionic and Electronic Conduction in TiNb₂O₇, 141 (2019) 16706–16725. <https://doi.org/10.1021/jacs.9b06669>.
- [16]



L. Hu, L. Luo, L. Tang, C. Lin, R. Li, Y. Chen, Ti₂Nb₂xO₄+5x anode materials for lithium-ion batteries: a comprehensive review, 6 (2018) 9799–9815. <https://doi.org/10.1039/c8ta00895g>.

[17]

S. Lou, X. Cheng, Y. Zhao, A. Lushington, J. Gao, Q. Li, P. Zuo, B. Wang, Y. Gao, Y. Ma, C. Du, G. Yin, X. Sun, Superior performance of ordered macroporous TiNb₂O₇ anodes for lithium ion batteries: Understanding from the structural and pseudocapacitive insights on achieving high rate capability, 34 (2017) 15–25. <https://doi.org/10.1016/j.nanoen.2017.01.058>.

[18]

B. Guo, X. Yu, X. Sun, M. Chi, Z. Qian, J. Liu, Y. Hu, X. Yang, J. Goodenough, S. Dai, A long-life lithium-ion battery with a highly porous TiNb₂O₇ anode for large-scale electrical energy storage, 7 (2014). <https://doi.org/10.1039/c4ee00508b>.

[19]

Q. Cheng, J. Liang, Y. Zhu, L. Si, C. Guo, Y. Qian, Bulk Ti₂Nb₁₀O₂₉ as long-life and high-power Li-ion battery anodes, 2 (2014) 17258–17262. <https://doi.org/10.1039/c4ta04184d>.

[20]

R. Inada, T. Mori, R. Kumasaka, R. Ito, T. Tojo, Y. Sakurai, Characterization of vacuum-annealed TiNb₂O₇ as high potential anode material for lithium-ion battery, 16 (2019) 264–272. <https://doi.org/10.1111/ijac.13058>.

[21]

C. Lin, S. Yu, S. Wu, S. Lin, Z.-Z. Zhu, J. Li, L. Lu, Ru_{sub(0.01)Ti}sub(0.99)Nb_{sub(2)O}sub(7) as an intercalation-type anode material with a large capacity and high rate performance for lithium-ion batteries, 3 (2015) 8627–8635. <https://doi.org/10.1039/c5ta01073j>.

[22]

K.J. Griffith, A. Senyshyn, C.P. Grey, Structural Stability from Crystallographic Shear in TiO₂–Nb₂O₅ Phases: Cation Ordering and Lithiation Behavior of TiNb₂₄O₆₂, 56 (2017) 4002–4010. <https://doi.org/10.1021/acs.inorgchem.6b03154>.

[23]

R. Kodama, Y. Terada, I. Nakai, S. Komaba, N. Kumagai, Electrochemical and In Situ XAFS-XRD Investigation of Nb_{sub(2)O}_{sub(5)} for Rechargeable Lithium Batteries, 153 (2006). <https://doi.org/10.1149/1.2163788>.

[24]

N. Takami, K. Ise, Y. Harada, T. Iwasaki, T. Kishi, K. Hoshina, High-energy, fast-charging, long-life lithium-ion batteries using TiNb₂O₇ anodes for automotive applications, 396 (2018) 429–436. <https://doi.org/10.1016/j.jpowsour.2018.06.059>.

[25]

C. Yang, S. Deng, C. Lin, S. Lin, Y. Chen, J. Li, H. Wu, Porous TiNb₂₄O₆₂ microspheres as high-performance anode materials for lithium-ion batteries of electric vehicles, 8 (2016) 18792–18799. <https://doi.org/10.1039/c6nr04992c>.

[26]

C. Lin, S. Deng, D.J. Kautz, Z. Xu, T. Liu, J. Li, N. Wang, F. Lin, Intercalating Ti₂Nb₁₄O₃₉ Anode Materials for Fast-Charging, High-Capacity and Safe Lithium–Ion Batteries, 13 (2017) n/a. <https://doi.org/10.1002/sml.201702903>.

[27]

G. Wang, Z. Wen, L. Du, Y.-E. Yang, S. Li, J. Sun, S. Ji, Hierarchical Ti–Nb oxide microspheres with synergic multiphase structure as ultra-long-life anode materials for lithium-ion batteries, 367 (2017) 106–115. <https://doi.org/10.1016/j.jpowsour.2017.09.061>.

[28]

H. Park, T. Song, U. Paik, Porous TiNb₂O₇ nanofibers decorated with conductive Ti_{1–x}Nb_xN bumps as a high power anode material for Li-ion batteries, 3 (2015) 8590–8596. <https://doi.org/10.1039/c5ta00467e>.

[29]

R.D. Shannon, Revised effective ionic radii and systematic studies of interatomic distances in halides and chalcogenides, 32 (1976) 751–767. <https://doi.org/10.1107/S0567739476001551>.

[30]

X. Lu, Z. Jian, Z. Fang, L. Gu, Y.-S. Hu, W. Chen, Z. Wang, L. Chen, Atomic-scale investigation on lithium storage mechanism in TiNb₂O₇, 4 (2011) 2638–2644. <https://doi.org/10.1039/c0ee00808g>.

[31]

M.R. Lukatskaya, B. Dunn, Y. Gogotsi, Multidimensional materials and device architectures for future hybrid energy storage, 7 (2016). <https://doi.org/10.1038/ncomms12647>.

[32]

B. Zhao, R. Ran, M. Liu, Z. Shao, A comprehensive review of Li₄Ti₅O₁₂-based electrodes for lithium-ion batteries: The latest



advancements and future perspectives, 98 (2015) 1–71.
<https://doi.org/10.1016/j.mser.2015.10.001>.

View Article Online
DOI: 10.1039/D4TA08141B

[33]

H. Shim, E. Lim, S. Fleischmann, A. Quade, A. Tolosa, V. Presser, Nanosized titanium niobium oxide/carbon electrodes for lithium-ion energy storage applications, 3 (2019) 1776–1789.
<https://doi.org/10.1039/c9se00166b>.

[34]

Y. Son, J. Ma, N. Kim, T. Lee, Y. Lee, J. Sung, S. Choi, G. Nam, H. Cho, Y.J. Yoo, J. Cho, Quantification of Pseudocapacitive Contribution in Nanocage-Shaped Silicon–Carbon Composite Anode, 9 (2019).
<https://doi.org/10.1002/aenm.201803480>.

[35]

W.L. Wang, B.-Y. Oh, J.-Y. Park, H. Ki, J. Jang, G.-Y. Lee, H.-B. Gu, M.-H. Ham, Solid-state synthesis of Ti₂Nb₁₀O₂₉/reduced graphene oxide composites with enhanced lithium storage capability, 300 (2015) 272–278. <https://doi.org/10.1016/j.jpowsour.2015.09.078>.

[36]

J.T. Lee, C. Jo, M. DeVolder, Bicontinuous phase separation of lithium-ion battery electrodes for ultrahigh areal loading, 117 (2020) 21155–21161. <https://doi.org/10.1073/pnas.2007250117>.

[37]

C. Lin, S. Yu, S. Wu, S. Lin, Z.-Z. Zhu, J. Li, L. Lu, Ru_{0.01}Ti_{0.99}Nb₂O₇ as an intercalation-type anode material with a large capacity and high rate performance for lithium-ion batteries, 3 (2015) 8627–8635. <https://doi.org/10.1039/C5TA01073J>.

[38]

Z. Yao, X. Xia, S. Zhang, C. Zhou, G. Pan, Q. Xiong, Y. Wang, X. Wang, J. Tu, Oxygen defect boosted N-doped Ti₂Nb₁₀O₂₉ anchored on core-branch carbon skeleton for both high-rate liquid & solid-state lithium ion batteries, 25 (2020) 555–562.
<https://doi.org/10.1016/j.ensm.2019.09.027>.



The raw data supporting the findings of this study are available at the University of Cambridge's open data repository under DOI: <https://doi.org/10.17863/CAM.116030>.

[View Article Online](#)

DOI: 10.1039/D4TA08141B

Open Access Article. Published on 19 February 2025. Downloaded on 2/22/2025 6:04:27 AM.
This article is licensed under a Creative Commons Attribution 3.0 Unported Licence.

